Indian Journal of Natural Products and Resources
Vol. 17(2), June 2026, pp. 318-330
DOI: 10.56042/ijnpr.v17i2.21478

Chitosan-based nanogel of *Opuntia elatior* Mill.: Molecular docking, anti inflammatory, and wound healing efficacy

Tejaswini Magar[1], Diksha Desai[1], Shreya Todkar[1], Sandhya Giri[1], Karan Dongale[1], Pratik Maske[1]*, Shobhraj Malavi[2], Omkar Tipugade[3], Suraj Ambale[4] and Umesh Kolap[5]

[1]Department of Pharmaceutical Chemistry, [2]Department of Pharmaceutics, [4]Department of Pharmaceutical Quality Assurance, [5]Department of Biopharmaceutics, Genesis Institute of Pharmacy, Sonyachi Shiroli, Radhanagari, Maharashtra 416212, India

[3]Department of Pharmaceutics, Krishna Institute of Pharmacy, Krishna Vishwa Vidyapeeth (Deemed to be University), Karad, Maharashtra 415539, India

Received 10 July 2025; revised received 16 May 2026; accepted 25 May 2026

The existing study investigates the formulation and evaluation of a chitosan-based nanogel containing *Opuntia elatior* Mill. extract, aimed at enhancing anti-inflammatory and wound healing efficacy through both *in vitro* and *in silico* approaches. *O. elatior*, a xerophytic plant widely used in traditional medicine, is rich in bioactive compounds known for their therapeutic potential. Ionic gelation was used to incorporate the extract obtained by maceration into chitosan nanoparticles. These nanoparticles were further formulated into a nanogel using Carbopol 934. Dynamic light scattering (DLS) analysis of the produced nanogel showed a Z-average particle size of 89.34 nm, a polydispersity index (PDI) of 0.416, and a zeta potential of +14.1 mV, showing good stability and dispersibility. Characterisation techniques, including FTIR, SEM, DSC-TGA, and XRD, confirmed the presence and successful incorporation of the extract within the gel matrix. Protein denaturation and trypsin inhibition tests were used to assess the nanogel's *in vitro* anti-inflammatory activity, and the results showed it was either as effective as or more effective than diclofenac sodium. Wound-healing efficacy was evaluated using a scratch assay with L929 fibroblast cells, in which the nanogel promoted significant cell migration and wound closure. Furthermore, molecular docking studies showed strong binding affinities of key phytoconstituents, particularly isoquercetin, with TNF-alpha protein (PDB ID: 2AZ5), suggesting potential anti-inflammatory mechanisms. These results collectively indicate that the chitosan-based nanogel from *O. elatior* is a promising candidate for topical application to manage inflammation and promote wound healing, thereby validating its traditional medicinal use.

Keywords: Ligand, Maceration, Nanogel, *Opuntia elatior* Mill., Thermal analysis

IPC code; Int. cl. (2021.01)– A61K 36/00, A61K 36/33, A61K 131/00, A61P 17/00, A61P 29/00

Introduction

Prickly pears, or cactus pears, are members of the genus *Opuntia* and family Cactaceae. It has been used for centuries by ancient civilisations to treat various ailments and promote wound healing. The fruit comes in a variety of hues, such as orange-yellow, green, and purple-red[1] *Opuntia dillenii* Haw is one of the three main species found in India. *Opuntia vulgaris* Mill is found in southern regions. *O. elatior* Mill. is located in the north. In the western regions, especially in Saurashtra and Kutch[2]. *O. elatior* is a xerophytic shrub that is a member of the dicotyledonous angiosperm family Cactaceae, which has more than 1,500 species worldwide[3]. This species is especially abundant in the semi-arid regions of Saurashtra and northern Gujarat. Locally referred to as "Hathlo Thor," *O. elatior* is traditionally consumed as a juice for its medicinal benefits, particularly for maintaining healthy blood physiology[4].

Traditionally, *O. elatior* has been used by the tribal communities of Rajasthan to cure a health conditions, including wounds, gastric burning, abscesses, diphtheria, anaemia, hyperglycemia, hyperlipidemia, pain, inflammation, cancer, high cholesterol, ulcers, viral infections, asthma, cough, fever, gonorrhea, eye infections (ophthalmia), leukaemia, and as a diuretic, refrigerant, antileukemic, immunomodulator, neuroprotective agent, and monoamine oxidase inhibitor. It is also believed to improve platelet function and holds significant nutritional value. Flavonoids, carbohydrates, tannins, proteins, and pectin have all been identified through phytochemical studies; these components contribute to the plant's diverse pharmacological properties[5,6]. Although currently available anti-inflammatory and wound

*Correspondent author
Email: ppmaske.genesis@gmail.com

healing drugs are effective, they are often associated with significant side effects. In contrast, herbal products are generally perceived as safer due to their natural origin, highlighting the need to develop potent therapeutic agents with minimal adverse effects[7]. An essential physiological defence system, inflammation protects the body from allergies, burns, toxic chemicals, infections, and other damaging stimuli. However, unchecked or persistent inflammation can lead to the onset of several chronic diseases[8].

The wound healing process is a complex and highly coordinated sequence of events involving four overlapping and interdependent phases: hemostasis, inflammation, proliferation, and maturation/remodeling[9]. Von Will brand factor, which encourages platelet adhesion, aggregation, and activation, is released by endothelial cells immediately after injury, starting the haemostatic phase. Activated platelets release a range of mediators that facilitate fibrin clot formation, thereby sealing the wound and preventing further blood loss[10]. Concurrently, elevated calcium levels contribute to smooth muscle contraction, leading to vasoconstriction and reduced blood flow. This initial phase is short-lived, typically lasting only a few minutes. The inflammatory phase follows, characterised by the release of histamine and serotonin from mast cells, resulting in vasodilation and increased vascular permeability. This facilitates the recruitment of neutrophils and monocytes to the wound site, where they eliminate invading pathogens and cellular debris through phagocytosis. These immune cells then release cytokines that initiate the next stage of healing. This stage generally persists for 0-3 days[11]. The proliferative phase extends approximately from day 3 to day 12 and is marked by the formation of granulation tissue by fibroblasts, which supports keratinocyte migration and re-epithelialization. This phase also involves active angiogenesis to restore blood supply to the regenerating tissue. Macrophages and mast cells secrete several growth factors that further regulate tissue repair and vascular network formation[11]. The final stage, maturation or remodeling, involves collagen reorganisation and wound contraction. During this phase, myofibroblasts derived from fibroblasts play a key role in tissue contraction and structural remodeling, which may continue from several days to months. Scar maturation and increased tensile strength result from type I collagen eventually replacing type III collagen. This process is primarily regulated by transforming growth factor-beta (TGF-β); however, complete restoration of original skin architecture is not achieved, and the tensile strength typically reaches only about 80% of that of uninjured skin[9].

The therapeutic potential of natural products and phytoconstituents in improving wound regeneration through multi-target mechanisms has drawn more scientific interest in recent years. Plant-derived bioactive compounds such as flavonoids, phenolic acids, tannins, alkaloids, and terpenoids have demonstrated exceptional promise for wound healing due to their antioxidant, anti-inflammatory, antibacterial, and collagen-promoting properties[12]. These phytochemicals help scavenge reactive oxygen species, reduce oxidative stress at the wound site, regulate pro-inflammatory cytokines, and promote tissue regeneration and re-epithelialisation[13].

To prevent infection and facilitate rapid wound healing, various antibacterial drug delivery systems, such as hydrogels, nanogels, nanoparticles, nanofibers, films, and wound dressings, have been developed as effective wound management strategies. Because of their better physicochemical and biological properties compared to traditional micro- and macro-scale hydrogels, nanogels have become a particularly intriguing platform among them[14]. They exhibit excellent drug loading efficiency, enhanced permeability across biological membranes, high aqueous solubility, thermal stability, biocompatibility, and structural integrity[15]. Nanogels are hydrophilic polymeric networks crosslinked at the nanoscale and capable of absorbing significant volumes of water without losing their three-dimensional structure. Because of their special properties, they can keep the wound moist, which is essential for optimal cellular migration, tissue regeneration, and faster healing[16]. In comparison to conventional gel systems, nanogels provide several additional advantages, including a significantly higher surface area, improved drug encapsulation capacity, controlled and sustained drug release profiles, and enhanced penetration of bioactive molecules into deeper layers of the skin[17].

The current study aims to support the traditional therapeutic use of *O. elatior* by assessing its anti-inflammatory and wound-healing properties in nanogel form. Additionally, a computational molecular docking approach was employed to investigate the potential anti-inflammatory properties

of several phytoconstituents from *O. elatior* and to identify probable molecular mechanisms of action.

Materials and Methods

Chemical materials

Chitosan was procured from PR Media Laboratory Pvt. Ltd., Dalibagh, Lucknow, Uttar Pradesh, India. Loba Chemie Pvt. Ltd., located in Mumbai, Maharashtra, India, provided glacial acetic acid, calcium chloride, sodium hydroxide, Carbopol 934, propylene glycol, propyl paraben, methyl paraben, and triethanolamine. Research Lab Fine Chem Industries in Sangli, Maharashtra, India, provided the sodium alginate. Every chemical utilised in this investigation was of analytical grade.

Plant material

The fresh fruit of *O. elatior* was collected between January and February 2025 from local regions of Kolhapur, Maharashtra, India. A botanist, Ms. Sonali Kumbhar, Assistant Professor at Devchand College's Faculty of Botany in Arjunnagar, Maharashtra, verified the authenticity of the plant specimen (2024/Sr/Bot./OE-23). For extraction, the seeds and stalks were removed, and the fruits were homogenised using a laboratory-scale homogeniser[18].

Preparation of methanolic extract from fruits of *O. elatior*

Ethanolic extract of *O. elatior* fruits was prepared utilising the maceration method with slight modifications from previously reported procedures[19]. Fresh fruits were cleaned properly, chopped into small pieces, dried in the shade, and then ground into a coarse powder. After transferring 100 g of powdered material into an airtight glass container, enough 90% ethanol was added to fully submerge the plant material. To improve solvent penetration and extraction efficiency, the mixture was kept at room temperature for a whole day while being shaken periodically. To maximise the recovery of phytoconstituents, the extract was filtered after the first maceration, and the marc was then macerated again for an additional four days using a new solvent. A rotating vacuum evaporator was used to concentrate the mixed filtrates at low pressure to produce a semi-solid extract. The extract yield, expressed as a percentage, was determined to be 14.6% w/w. The yield percentage was calculated utilising the standard formula.

$$\text{Percentage Yield (\%)} = \frac{\text{Weight of dried extract}}{\text{Weight of crude drug}} * 100$$

Preparation of *O. elatior*-loaded chitosan nanoparticles

As previously described, the ionic gelation process was utilised to create chitosan nanoparticles loaded with an extract from *O. elatior*[20]. Briefly, 10 mg of chitosan powder was dissolved in a 1% (w/v) glacial acetic acid solution, continuously stirred magnetically at 500 rpm for three hours. The chitosan solution was then combined with 100 µL of *O. elatior* extract to create a clear, brownish slurry. To create the nanoparticles, 10 mL of the chitosan extract solution was mixed with 5 mL of sodium tripolyphosphate (TPP) solution dropwise, while continuously stirring for an additional half hour. After that, the chitosan suspension was ultrasonicated for five minutes at a 40% amplitude. Ultra-centrifugal filters were used to gather the freshly made nanoparticles, which were then freeze-dried.

Formulation of the nano-sized topical gel

The nano-sized topical gel was prepared using the previously mentioned cold mechanical technique[21]. Carbopol 934 was used as the gelling agent. Briefly, 1.5 g of Carbopol 934 was gradually sprinkled into 80 mL of deionised water under continuous stirring to prevent lump formation and achieve uniform dispersion of the polymer. The dispersion was allowed to stand overnight to ensure complete hydration and swelling of the polymer chains, which facilitated the formation of a homogeneous gel matrix. The use of deionised water provided an ion-free medium, minimising undesirable interactions with the polymer and promoting stable nanogel formation. Subsequently, chitosan nanoparticles loaded with *O. elatior* extract were incorporated into the hydrated gel base at a concentration of 16 mg/mL. Glycerol (2 g) was then added as a humectant to improve consistency and spreadability, while methylparaben was incorporated as a preservative. Finally, volume was adjusted to 100 mL utilising deionised water to obtain the desired nano-sized topical gel formulation.

Characterisation of nanogel

Fourier Transform Infrared Spectroscopy (FTIR)

The distinctive functional groups in the *O. elatior* extract and chitosan nanoparticles loaded with *O. elatior* extract nanogels were identified utilising FTIR analysis. Each sample was finely mixed with potassium bromide (KBr) powder and compressed into pellets before analysis. The spectra were recorded within the frequency range of 400-4000 cm^{-1}(Ref.22).

Evaluation of nanogel

Studies on pH, physical characteristics, viscosity, spreadability, *in vitro* release, and stability were carried out in compliance with ICH criteria[23]. A Brookfield viscometer with spindle number six was utilised to measure the viscosity of the nanogel. According to ICH stability guidelines, formulations were stored in scintillation glass vials and incubated under three distinct conditions for three months: 4±2°C/60%±5% RH, 25±2°C/65%±5% RH, and 40±2°C/75%±5% RH. To ensure accuracy and repeatability, every assessment, including pH, physical appearance, viscosity, and spreadability, was carried out in triplicate[24,25].

Particle size, polydispersity index, and zeta potential

Particle size and PDI of the nanogels were determined by suspending the samples in ultra-pure water[26]. An appropriate volume of the suspension was transferred to a cuvette, any air bubbles removed, and the cuvette was placed into the Zetasizer for measurement. The DLS method, which analyses the Brownian motion of particles and determines their size using existing models, was utilised for the analysis[27]. The samples were diluted with 0.1 mM potassium chloride for zeta potential analysis and placed in an electrophoretic cell under a 15 V/cm electric field to measure surface charge[28].

Thermal analysis

Differential Scanning Calorimetry (DSC) and Thermogravimetric Analysis (TGA) were utilised to assess the thermal stability of the components in the developed formulations. DSC was conducted over a temperature range of 25-400°C with a heating rate of 10°C/min and a constant nitrogen flow of 10 mL/min, while TGA was conducted from 25-600°C under an inert nitrogen atmosphere. All samples were examined in triplicate[29]. The initial decomposition temperature and residual mass % were ascertained utilising the TGA thermograms. Furthermore, the DTA curve's differential peaks were used to calculate the nanogels' maximum thermal breakdown temperature[30].

X-ray Diffraction (XRD) analysis

XRD analysis was performed on chitosan nanoparticles loaded with *O. elatior* extract nanogels to assess their crystalline nature. The diffraction pattern was acquired over a 2θ range of 10–60° at a scanning rate of 1° 2θ/min at 25°C after powdered solid samples were put in the sample holder[31].

Scanning Electron Microscopy (SEM)

The morphology and surface texture of chitosan nanoparticles containing *O. elatior* extract nanogels were analysed utilising SEM. After drying and powdering the nanogel, it was sonicated for 10 minutes to disperse it in water at a concentration of 1 mg/mL. After casting the resultant dispersion onto a glass slide, it was allowed to dry. SEM was used to examine the form and surface properties at an acceleration voltage of 10 kV[32].

Inhibition of proteins denaturation

Briefly, the reaction mixture consisted of 4 mL of nanogel solution (250, 500, and 1000 µg/mL) or the reference drug diclofenac sodium at the same concentrations, mixed with 5.6 mL of phosphate-buffered saline (PBS, pH 6.4) and 0.4 mL of egg albumin obtained from a fresh hen's egg. The mixture was incubated at 37±2°C for 15 minutes, followed by heat-induced denaturation in a water bath at 70°C for 10 minutes. After cooling, the absorbance was measured at 660 nm using a Shimadzu UV spectrophotometer[33]. Protein stabilisation, or the prevention of heat-induced albumin denaturation, was demonstrated by an increase in absorbance of the test samples (As) relative to the control (Ac). After that, the % inhibition of protein denaturation was computed.

$$\text{Inhibition (\%)} = \frac{\text{As}-\text{Ac}*100}{\text{Ac}}$$

Trypsin inhibitory assay using bovine serum albumin (BSA)

The reaction mixture consisted of 300 µL of nanogel at varying concentrations (250, 500, and 1000 µg/mL) dissolved in distilled water, 300 µL of 0.5 µL trypsin solution, 100 µL of test sample at the respective concentrations, and 100 µL of 1% BSA solution. The final volume was adjusted to 300 µL using Tris-HCl buffer. The mixture was incubated at 37 °C for 20 minutes. The reaction was terminated by adding 0.5 µL of 0.1 N hydrochloric acid. Following this, the samples were centrifuged at 5000 rpm for 5 minutes, and the absorbance of the supernatant was measured at 280 nm using a UV-VIS spectrophotometer[34,35]. The reference standard was diclofenac. The following formula was utilised to determine the percentage of protease inhibition by the nanogel and diclofenac.

$$\text{Protease inhibition (\%)} = \frac{1 - \text{At} * 100}{\text{Ac}}$$

where At is the absorbance of the test sample, and Ac is the absorbance of the control.

Scratch Assay

The wound-healing potential of the sample was evaluated using an *in vitro* cell migration assay with L929 fibroblast cells, following a previously established protocol. L929 cells were seeded at a density of 2 × 10^5 cells/mL into 6-well plates containing DMEM supplemented with 10% fetal bovine serum (FBS) and incubated overnight at 37°C in a humidified atmosphere of 5% CO_2. After incubation, the culture medium was aspirated, and a uniform scratch was made across the cell monolayer using a sterile yellow pipette tip. Detached cells and debris were removed by washing with Dulbecco's phosphate-buffered saline (DPBS). The scratched cell monolayers were then treated with 100 µL of the sample (Curcumin) and 5 µg/mL of Cipladine, a standard drug known for its wound healing properties. Untreated cells served as the negative control. Following treatment, cells were incubated for 12 hours at 37°C in a 5% CO_2 humidified incubator[36,37]. An inverted microscope with a digital camera was utilised to view and record cell migration and morphological changes. SAGLO software was utilised to quantitatively analyse the scratch width and percentage of wound closure after 48 hours, after the assay was carried out in triplicate (n = 3).

Molecular docking studies

Ligand preparation

The interactions between the phytoconstituents of *O. elatior* were examined using molecular docking. and the target protein linked to rheumatoid arthritis. Following preparation and energy minimisation, the 2D structures of the specific phytoconstituents used as ligands were obtained from the PubChem database in .sdf format[38].

Preparation of macromolecule

The RCSB Protein Data Bank provided the crystal structure of the TNF-alpha protein complexed with a small molecule inhibitor (PDB ID: 2AZ5)[39]. Using Molsoft ICM Pro, the protein structure was generated by adding hydrogen atoms, removing water molecules, assigning partial charges, determining the correct protonation states, and applying the required structural constraints[40]. The active binding sites were found after the co-crystallised ligand was removed, and a grid box was created to specify the docking region for further molecular docking investigations[41].

Ligand–protein docking

The Glide module of Molsoft ICM Pro was used to dock each bioactive compound to the specified binding site within the defined grid. This software is a fast, efficient molecular docking tool specifically developed to predict the binding orientation of small molecules within receptor active sites. Its scoring system utilises van der Waals forces, shape complementarity, and electrostatic interactions to assess ligand-receptor interactions. The key active-site interactions, along with their corresponding docking scores, were systematically analysed and interpreted[42,43].

Results and Discussions

FTIR

The functional groups of the *O. elatior* extract were identified, and their retention in the nanogel formulation was confirmed using FTIR spectroscopy. A large absorption band about 3400 cm^{-1} in the extract's FTIR spectrum (Fig. 1a) corresponded to O-H stretching vibrations, suggesting the presence of hydroxyl-containing chemicals like polyphenols. Peaks observed at 2920-2850 cm^{-1} were attributed to C-H stretching of aliphatic hydrocarbons, while a

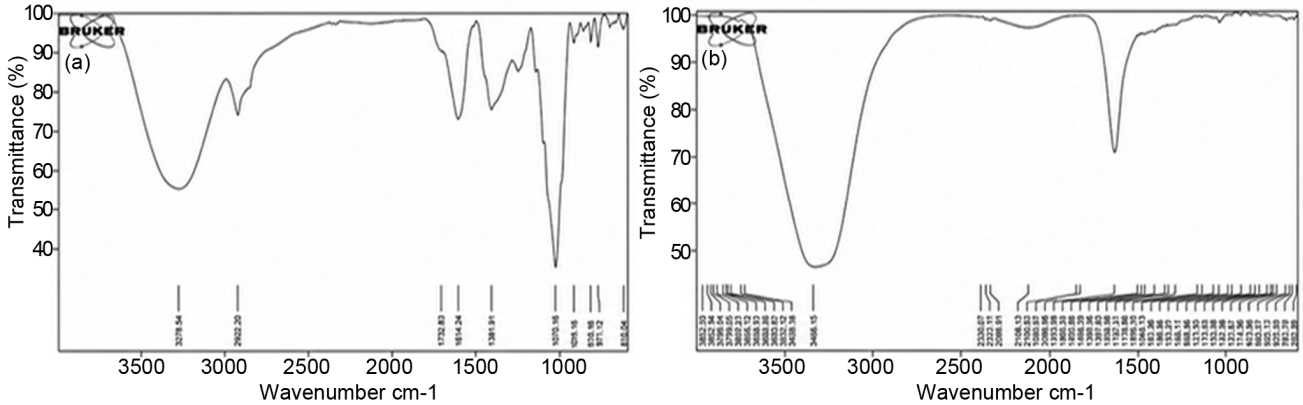

Fig. 1 — (a) FTIR of *Opuntia elatior* Mill. Extract, and (b) FTIR of *Opuntia elatior* Mill. Nanogel.

distinct peak near 1720 cm^{-1} suggested the presence of carbonyl (C=O) groups, likely from esters or carboxylic acids. Additionally, peaks around 1600-1650 cm^{-1} indicated C=C stretching vibrations of aromatic rings or amide groups, and the absorption in the range of 1000-1300 cm^{-1} was associated with C-O stretching vibrations from ethers or polysaccharides. The FTIR spectrum of the *O. elatior* nanogel (Fig. 1b) showed similar characteristic peaks, confirming the successful incorporation and retention of the major functional groups of the plant extract in the gel matrix. The slight shifts and broadening of some peaks in the nanogel spectrum further suggest possible interactions between the phytoconstituents and the gel-forming agents.

Evaluation of nanogel

The prepared chitosan-based *O. elatior* nanogel was evaluated for its physical appearance, pH, spreadability, and viscosity, as presented in Table 1. The nanogel exhibited a slightly yellowish tint and a smooth, transparent appearance. The pH was measured at 6.5 (in triplicate). The spreadability of the formulation was determined to be 23.3±0.3535 g·cm/sec, while the viscosity was recorded as 2058 cps.

Stability studies

The stability of chitosan-based *O. elatior* nanogel formulations was evaluated over 3 months under different storage conditions: 4±2°C/60±5% RH, 25±2°C/60±5% RH, and 40±2°C/65±5% RH. Physical appearance, viscosity, pH, and spreadability were evaluated for the formulations; the latter three parameters were examined three times. At refrigerated conditions (4±2°C/60±5% RH), the nanogels remained stable with no significant changes observed in physical appearance, pH, spreadability, or viscosity throughout the 90-day study period (Table 2). However, at room temperature (25±2°C/60±5% RH), minor changes in these parameters were noted (Table 2). In contrast, formulations stored at elevated temperature (40±2°C/65±5% RH) exhibited pronounced changes in physical appearance, pH, drug content, spreadability, and viscosity (Table 2). These results indicate that refrigerated conditions (4±2°C/60±5% RH) provide optimal stability for chitosan-based *O. elatior* nanogel formulations.

Particle size, polydispersity index, and zeta potential

The chitosan-based nanogel of *O. elatior* showed a Z-average particle size of 89.34 nm (Fig. 2a), a dominant peak at 210.7 nm, and a PDI of 0.416, indicating a moderately polydisperse nanoscale system suitable for drug delivery and wound healing. The zeta potential was +14.1 mV (Fig. 2b), suggesting moderate colloidal stability and good bioadhesive and antimicrobial properties due to chitosan, supporting its anti-inflammatory and wound-healing potential.

Thermal analysis

The DSC-TGA analysis of the gel sample showed a major weight loss of 92.71%, suggesting a high rate of evaporation of volatile substances such as water or organic solvents. A sharp endothermic peak was observed (Fig. 3a) at 40.23°C with an enthalpy of 1140 J/g. A secondary thermal event occurred at 67.71°C, possibly indicating a glass transition or further minor phase change. The minimal residue of 0.1884% suggests negligible inorganic content. DTA analysis identified thermal transitions at peaks (Fig. 3b) at approximately 35.97 and 67.46°C, confirming the thermal events. Results indicate that the gel is thermally sensitive and must be stored below 40°C to maintain stability. The DSC-TGA analysis of the nanogel revealed significant weight loss (92.71%), primarily attributed to evaporation of water and volatile components, along with low-temperature endothermic transitions. Similar thermal behaviour has been reported for hydrogel and nanogel systems where high moisture content and polymeric network flexibility contribute to early thermal transitions and weight loss below 100°C, which is typical of chitosan-based systems used in topical delivery applications[44,45].

XRD analysis

To investigate the sample's crystalline characteristics, XRD analysis was performed. The diffractogram's

Table 1 — Evaluation parameters for nanogel formulation

S. No.	Nanogel	Physical appearance	pH	Spreadability (g.cm/sec)	Viscosity (cps)
1	Control-Nanogel	White, smooth, clear, and transparent	6.1	21.8±0.5824	2269
2	Chitosan-based *O. elatior* nanogel	Slight yellowish tint, smooth, clear, transparent	6.5	23.3±0.3535	2058

Table 2 — Stability studies

S.No.	Nanogel	Physical appearance	pH	Spreadability (g.cm/s)	Viscosity (cps)
		4 ± 2 °C/60 ± 5% RH for 3 Months			
1	Control-Nanogel	White, smooth, clear, and transparent	6.2	21.1±0.5824	2270
2	Chitosan-based *O. elatior* nanogel	Slight yellowish tint, smooth, clear, transparent	6.4	23.8±0.3535	2056
	25 ± 2 °C/60 ± 5% RH for 3 Months				
3	Control-Nanogel	White, smooth, clear, and transparent	6.6	20.1±0.5824	2275
4	Chitosan-based *O. elatior* nanogel	Slight yellowish tint, smooth, clear, transparent	6.9	20.3±0.3535	2060
	40 ± 2 °C/65 ± 5% RH for 3 Months				
5	Control-Nanogel	White, smooth, clear, and transparent	6.4	19.1±0.5824	2278
6	Chitosan-based *O. elatior* nanogel	Slight yellowish tint, smooth, clear, transparent	6.5	20.3±0.3535	2062

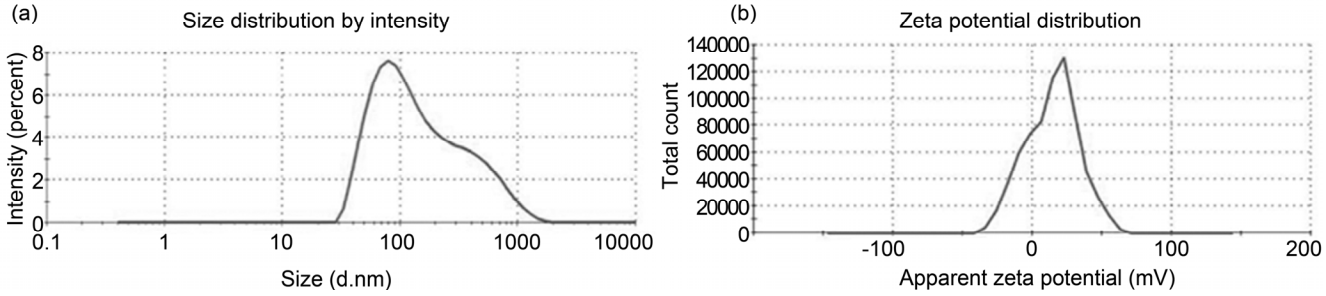

Fig. 2 — (a) Particle size of Chitosan-based *Opuntia elatior* Mill. Nanogel, and (b) Zeta Potential of Chitosan-based *Opuntia elatior* Mill. Nanogel.

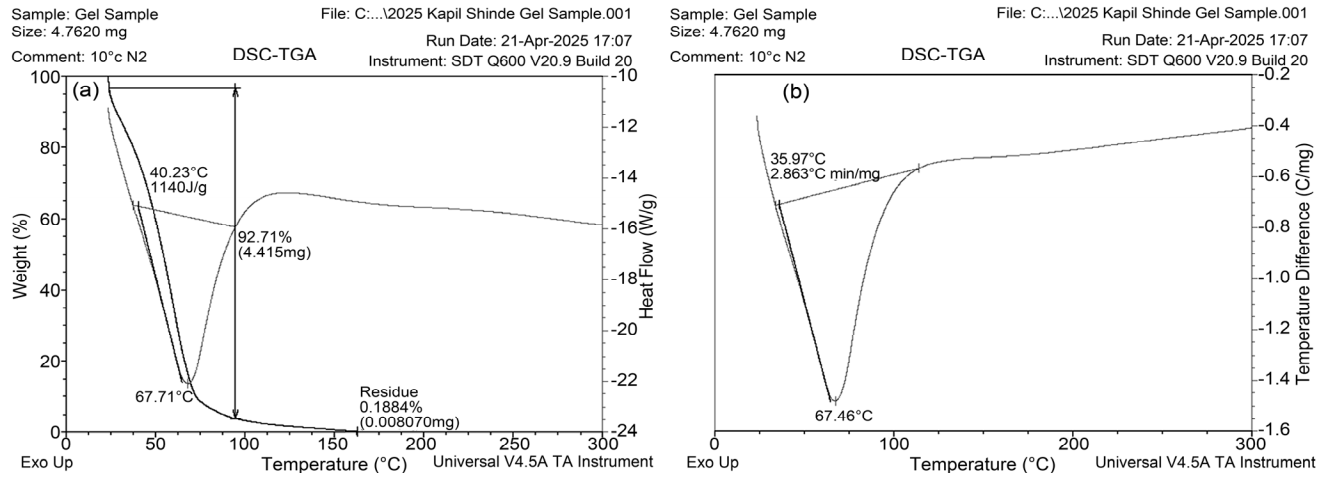

Fig. 3 — (a) DSC-TGA of Chitosan-Based Nanogel of *Opuntia elatior* Mill., and (b) DSC-TGA of Chitosan-Based Nanogel of *Opuntia elatior* Mill.

wide, dispersed peaks showed that the polymeric nanogel matrix was primarily amorphous. This amorphous behaviour is attributed to the gel formulation. Furthermore, the absence of characteristic crystalline peaks of the pure extract in the nanogel confirms the successful and uniform encapsulation of the drug within the amorphous polymeric network (Fig. 4). This is consistent with earlier studies reporting that incorporation of phytoconstituents into polymeric carriers leads to conversion from crystalline to amorphous form due to molecular dispersion, thereby improving solubility and bioavailability of active compounds[46,47].

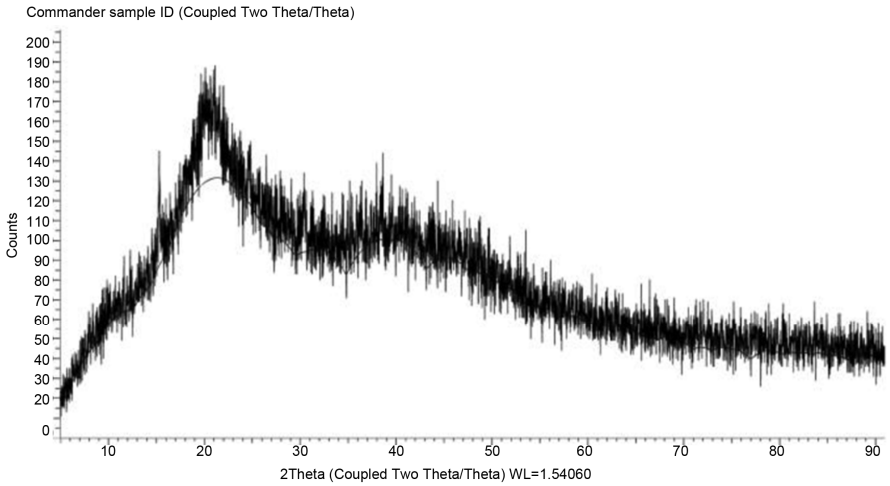

Fig. 4 — XRD of Chitosan-Based Nanogel of *Opuntia elatior* Mill.

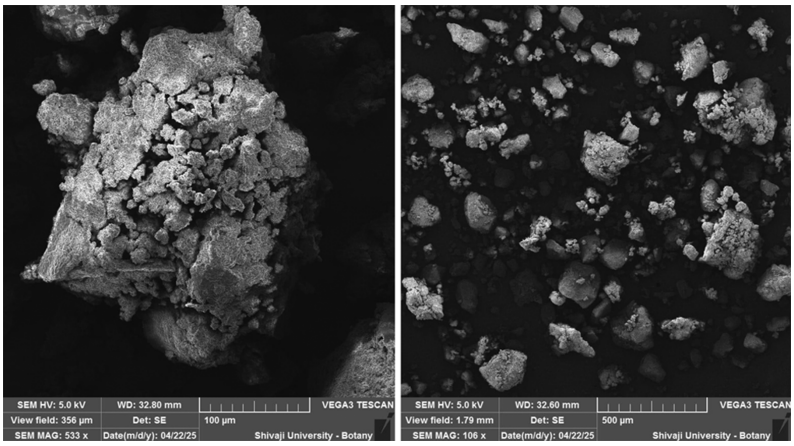

Fig. 5 — SEM of Chitosan-Based Nanogel of *Opuntia elatior* Mill.

SEM

Surface morphology and particle distribution of the nanogel were analysed utilising Scanning SEM at magnifications of 106× and 533×. The SEM images (Fig. 5) revealed that the nanogel particles possess a rough, irregular surface with noticeable aggregation. At lower magnification (106×), the particles were uniformly dispersed and exhibited a range of sizes. At higher magnification (533×), the surface appeared more textured, showing clusters of smaller particles adhered to larger agglomerates. This structural arrangement suggests the presence of porosity and a high surface area, both of which are advantageous for efficient drug loading and controlled release. Similar morphological characteristics have been reported in chitosan-based nanogels and hydrogel systems, where porosity enhances drug loading capacity, facilitates sustained release, and promotes fibroblast adhesion and migration, which are critical for wound-healing applications[48,49].

Inhibition of proteins denaturation

Inflammation is commonly associated with symptoms such as pain and elevated temperature, and is characterised by protein denaturation, increased membrane permeability, and alterations in vascular integrity[50]. Protein denaturation involves complex molecular interactions, including the disruption of electrostatic, hydrogen, hydrophobic, and disulfide bonds[51]. Utilising heat-induced denaturation of egg albumin as a model, the current study employed the protein denaturation inhibition technique to assess the formulation's anti-inflammatory potential. The effect of the chitosan-based nanogel loaded with *O. elatior* extract on protein denaturation is illustrated in the corresponding Fig. 6.

The results showed that both the nanogel and the standard drug inhibited protein denaturation in a concentration-dependent way. The nanogel showed percentage inhibitions of 81.05, 88.96, and 93.45% at doses of 250, 500, and 1000 µg, respectively. In

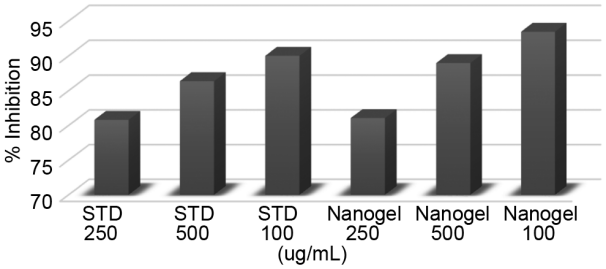

Fig. 6 — Effects of Chitosan-Based Nanogel of *Opuntia elatior* Mill. on Protein Denaturation.

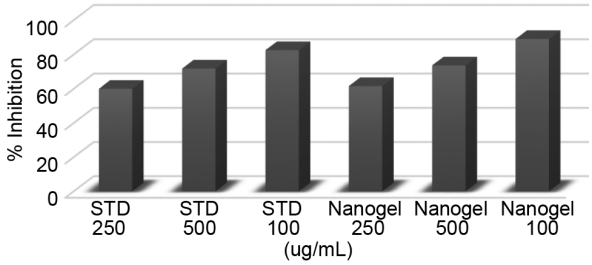

Fig. 7 — Effect of Chitosan-Based Nanogel containing *Opuntia elatior* Mill. on BSA denaturation.

Table 3 — Percentage of cells migrated towards the wound and involved in wound closure

Sample	Reading 0 Hrs (mm)	Mean	Reading 48 h (mm)	Mean	% of cell reduction
Control	10.00	10.01	9.79	9.76	
	09.98		9.80		
	10.05		9.70		
Standard-Cipladine 5µg/mL	10	10.01	1.22	1.22	87.53
	09.98		1.20		
	10.05		1.24		
Nanogel	10.00	10.01	2.90	2.90	70.59
	09.98		3.00		
	10.05		2.80		

comparison, diclofenac sodium showed 80.8%, 86.36%, and 90% inhibition at the same concentrations. The nanogel formulation displayed slightly higher efficacy than the standard, particularly at the highest concentration tested. The combination of biocompatible and stabilising qualities of chitosan nanoparticles with the synergistic anti-inflammatory qualities of *O. elatior* bioactive components may be responsible for this increased activity. This finding aligns with previous studies reporting that chitosan-based nanocarriers loaded with plant extracts exhibit enhanced anti-inflammatory activity due to synergistic interactions between the polymer and phytoconstituents. Chitosan is known to stabilise biological membranes and modulate inflammatory mediators, while flavonoids and phenolics contribute through antioxidant and cytokine-regulating effects[52].

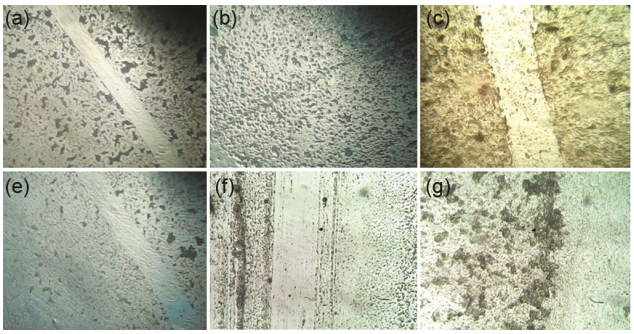

Fig. 8 — Microscopy images of L929 fibroblast cells migration after scratch. (a) Standard – Wound scratch (Cipladine), (b) After 48 Hours Standard-(Cipladine), (c) Control -Wound Scratch, (d) After 48 Hours-Control, (e) Nanogel wound scratch, and (f) Nanogel After 48 Hours.

Trypsin inhibitory assay using bovine serum albumin (BSA)

The anti-inflammatory potential of the chitosan-based nanogel containing *O. elatior* extract was evaluated through *in vitro* assays targeting key mechanisms involved in chronic inflammatory conditions such as rheumatoid arthritis (RA). These included the inhibition of protein denaturation and protease activity. The efficacy of the nanogel to prevent heat-induced denaturation, a process strongly associated with inflammation, was evaluated using a protein denaturation experiment with bovine serum albumin (BSA). With percentage inhibition values of 61.53, 73.58, and 88.96% at 250, 500, and 1000 µg/mL, respectively, the nanogel showed concentration-dependent inhibition of protease activity. In comparison, standard diclofenac sodium showed inhibition values of 59.93, 71.73, and 82.45% at the corresponding concentrations (Fig. 7). These results suggest that the nanogel formulation not only matches but surpasses the standard drug at higher concentrations, indicating a strong potential for protease inhibition.

Scratch assay

Using an *in vitro* scratch test with L929 fibroblast cells, the chitosan-based nanogel containing *O. elatior* extract was evaluated for its capacity to promote wound healing. A sterile scratch was introduced into a confluent monolayer of cells, and the nanogel (1000 µg/mL) was applied to assess its effect on cell migration and wound closure over 48 hours. The assay results demonstrated that the nanogel significantly promoted cell migration, achieving 70.59% wound closure, compared to 87.53% observed with the standard drug Cipladine (5 µg/mL), and only 2.49% in the untreated control group (Table 3, Fig. 8). These findings suggest that the

nanogel formulation facilitates cell proliferation and migration, contributing to wound repair.

Molecular docking studies

Eleven phytochemicals from *O. elatior* were used in molecular docking research as ligands and targeting a single macromolecule: a small-molecule inhibitor complexed with the TNF-alpha protein (PDB ID: 2AZ5). Docking simulations were performed using Molsoft ICM Pro to evaluate binding conformations and affinities. Among the tested compounds, isoquercetin showed the strongest binding affinity (-21.24 kcal/mol) with the target macromolecules. Additionally, ß-sitosterol, gallic acid, 6-Hydroxymethyl-4-methoxy-2H-pyran-2-one, Eicosadienoic acid, Palmitic acid, Arabinose, Betanine, Linoleic acid, Galactose, Stearic acid exhibited comparatively lower binding affinities than isoquercetin against the TNF-alpha protein complexed with a small molecule inhibitor (PDB ID: 2AZ5). Visual inspection confirmed that all ligands were successfully accommodated within the binding site of PDB: 2AZ5, as illustrated in the 3D molecular visualisation (Fig. 9). Molecular docking revealed that all compounds from *O. elatior* displayed favourable binding interactions with the TNF-alpha protein complexed with a small molecule inhibitor (PDB ID: 2AZ5). A summary of the binding affinities, identified binding pockets, and key ligand–receptor interactions is provided in the accompanying Table 4. The 3D visualisation (Fig. 10) confirms that all

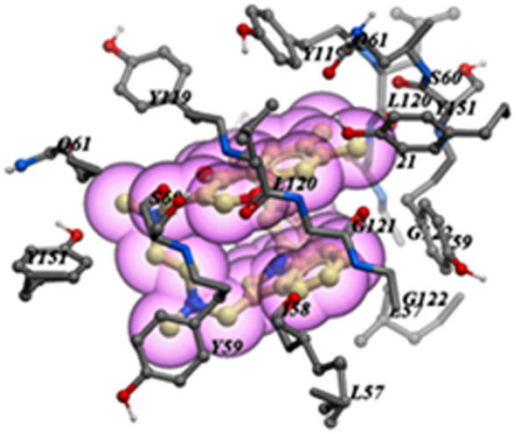

Fig. 9 — Identified Binding Pocket in PDB: 2AZ5.

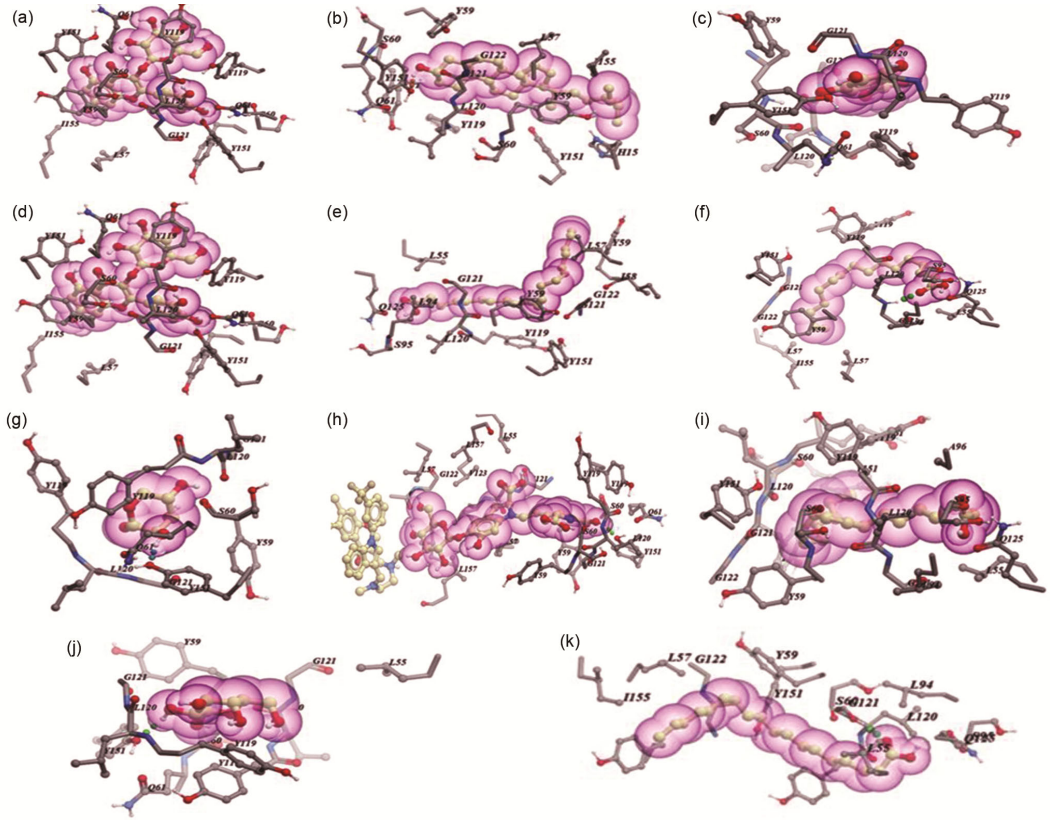

Fig. 10 — 3D View of Ligand Binding in the Binding Cavity. (a) Isoquercetin, (b) ß-sitosterol, (c) Gallic acid, (d) 6-Hydroxymethyl-4-methoxy-2H-pyran-2-one, (e) Eicosadienoic acid, (f) Palmitic acid, (g) Arabinose, (h) Betanine, (i) Linoleic acid, (j) Galactose, (k) Stearic acid with 2AZ.

Table 4 — Molsoft ICM Pro Docking score (kcal/mol) of *Opuntia elatior* Mill. Compounds against TNF-alpha protein complexed with a small molecule inhibitor (PDB ID: 2AZ5)

Name of the Compound	Dock Score	H Bond Score	Lipophilic Score
Isoquercetin	-21.24	-2.369	-4.214
ß-sitosterol	-18.22	-1.882	-7.624
gallic acid	-15.91	-2.924	-1.58
6-Hydroxymethyl-4-methoxy-2H-pyran-2-one	-15	-2.555	-3.03
Eicosadienoic acid	-14.35	-0.95	-6.887
Palmitic acid	-13.91	-2.636	-6.401
Arabinose	-13.72	-3.842	-2.031
Betanine	-12.36	-3.05	-5.95
Linoleic acid	-11.36	-3.884	-5.438
Galactose	-10.2	-3.423	-1.872
Stearic acid	-7.204	0	-7.313

compounds were successfully docked within the predicted binding sites.

Conclusion

This research demonstrates the potential of a chitosan-based nanogel loaded with *O. elatior* extract as an effective topical formulation for anti-inflammatory and wound-healing applications. The nanogel demonstrated favourable physicochemical properties essential for cutaneous application and bioavailability, including nanoscale particle size, moderate polydispersity, and positive zeta potential. The successful integration and compatibility of plant bioactive compounds within the chitosan gel matrix were validated through characterisation investigations. According to biological tests, the nanogel significantly reduced trypsin activity and protein denaturation in a concentration-dependent way, frequently outperforming the common medication diclofenac sodium. Additionally, the scratch assay confirmed its significant wound-healing potential by accelerating fibroblast migration. The molecular docking analysis supported these findings, with isoquercetin showing the highest binding affinity to the inflammatory mediator TNF-alpha, indicating a plausible mechanism for its observed effects. Overall, this study supports the traditional claims of *O. elatior* as a natural remedy and demonstrates its potential as a novel herbal nanogel for managing inflammation and enhancing wound repair.

Conflict of interest

The authors declare that there is no conflict of interest.

AI use disclosure

The authors declare that artificial intelligence (AI) tools were used solely for language improvement, grammar checking, and manuscript formatting assistance. All scientific content, data interpretation, analysis, conclusions, and final manuscript preparation were performed and verified by the authors, who take full responsibility for the content of the manuscript.

References

1 Scarano P, Naviglio D, Prigioniero A, Tartaglia M, Postiglione A, *et al*.., Sustainability: Obtaining natural dyes from waste matrices using the prickly pear peels of *opuntia ficus-indica* (l.) Miller, *Agronomy*, 2020, 10(4), 528, doi: 10.3390/agronomy10040528.

2 Kathiriya M R, Vekariya Y and Hati S, Exploring the biofunctionalities of lactic fermented cactus pear (*Opuntia elatior* Mill.) fruit beverage: an exotic superfood, *J Food Sci Technol*, 2024, 61(5), 969-982, doi: 10.1007/s13197-023-05893-y.

3 Itankar P, Sontakke V, Tauqeer M and Charde S, Antioxidant potential and its relationship with polyphenol content and degree of polymerization in *Opuntia elatior* Mill. fruits, *AYU (An Int Q J Res Ayurveda)*, 2014, 35(4), 423, doi: 10.4103/0974-8520.159010.

4 Patel F, Upadhyay K, Mammen D, Robin E, Ramachandran A V, *et al.*, Phytochemical composition and antiproliferative activity of *Opuntia elatior* Mill.: *In vitro* and *in silico* studies on breast cancer cell line MCF-7, *J Appl Biol Biotechnol*, 2023, doi: 10.7324/JABB.2024.144233.

5 Kumar P and Goyal G J, *In-vitro* and *in-vivo* antioxidant and anti-diabetic evaluation of cladodes crude extract and solvent fractions of *Opuntia elatior* Mill. (Cactaceae), *Int J Pharmacogn*, 2021, 8(6), 257-265, doi: 10.13040/IJPSR. 0975-8232.IJP.8(6).257-65.

6 Gouws C A, Georgousopoulou E N, Mellor D D, McKune A and Naumovski N, Effects of the consumption of prickly pear cacti (opuntia spp.) and its products on blood glucose levels and insulin: A systematic review, *Medicina (Kaunas)*, 2019, 55(5), doi: 10.3390/ medicina55050138.

7 Alqasoumi S I, Anti-inflammatory and wound healing activity of *Fagonia schweinfurthii* alcoholic extract herbal gel on albino rats, *Afr J Pharm Pharmacol*, 2011, 5(17), doi: 10.5897/AJPP11.190.

8 Chen L, Deng H and Cui H, Inflammatory responses and inflammation-associated diseases in organs, *Oncotarget*, 2018, 9(6), 7204-7218, doi: 10.18632/oncotarget. 23208.

9 Algül D, Kılıç E, Özkan F and Yağan U Y, Wound healing effects of new cream formulations with herbal ingredients, *Pharmaceutics*, 2025, 17(7), 941, doi: 10.3390/pharmaceutics17070941.

10 Reininger A J, Function of von Willebrand factor in haemostasis and thrombosis, *Haemophilia*, 2008, 14(s5), 11-26, doi: 10.1111/j.1365-2516.2008.01848.x.

11 Landén N X, Li D and Ståhle M, Transition from inflammation to proliferation: A critical step during wound healing, *Cell Mol Life Sci*, 2016, 73(20), 3861-3885, doi: 10.1007/s00018-016-2268-0.

12 Cedillo C M, Martinez L R, López J A M, López I L, Escutia-Perez S, *et al.*, Use of medicinal plants in the process of wound healing: A literature review, *Pharmaceuticals*, 2024, 17(3), 303, doi: 10.3390/ph17030303.

13 Ukaegbu K, Allen E and Svoboda K K H, Reactive oxygen species and antioxidants in wound healing: Mechanisms and therapeutic potential, *Int Wound J*, 2025, 22(5), doi: 10.1111/iwj.70330.

14 Hamidi M, Azadi A and Rafiei P, Hydrogel nanoparticles in drug delivery, *Adv Drug Deliv Rev*, 2008, 60(15), 1638-1649, doi: 10.1016/j.addr.2008.08.002.

15 Shoukat H, Pervaiz F and Khan M, Development of β-cyclodextrin/polyvinypyrrolidone-co-poly (2-acrylamide-2-methylpropane sulphonic acid) hybrid nanogels as nano-drug delivery carriers to enhance the solubility of Rosuvastatin: An *in vitro* and *in vivo* evaluation, *PLoS One*, 2022, 17(1), e0263026, doi: 10.1371/journal.pone.0263026.

16 Das T, Das M, Sultana S and Swain R, Stimuli-responsive nanogels in wound care: A comprehensive review, *Next Nanotechnol*, 2025, 8, 100260, doi: 10.1016/j.nxnano.2025.100260.

17 Manimaran V, Nivetha R P and Tamilanban T, Nanogels as novel drug nanocarriers for CNS drug delivery, *Front Mol Biosci*, 2023, 10, doi: 10.3389/fmolb.2023.1232109.

18 Alifakı Y Ö, Şakıyan Ö and Isci A, Extraction of phenolic compounds from cranberrybush (*Viburnum opulus* L.) fruit using ultrasound, microwave, and ultrasound-microwave combination methods, *J Food Meas Charact*, 2022, 16(5), 4009-4024, doi: 10.1007/s11694-022-01498-9.

19 Nofita S D, Ngibad K and Rodli A F, Determination of percentage yield and total phenolic content of ethanol extract from purple passion (*Passiflora edulis* f. edulis Sims) fruit peel, *J Pijar Mipa*, 2022, 17(3), 309-313, doi: 10.29303/jpm.v17i3.3461.

20 Alqahtani M S, Al-Yousef H M and Alqahtani A S, Preparation, characterization, and *in vitro-in silico* biological activities of *Jatropha pelargoniifolia* extract loaded chitosan nanoparticles, *Int J Pharm*, 2021, 606, 120867, doi: 10.1016/j.ijpharm.2021.120867.

21 Tan Y Y, Wong L S and Nyam K L, Development and evaluation of topical zinc oxide nanogels formulation using *Dendrobium anosmum* and its effect on acne vulgaris, *Molecules*, 2023, 28(19), 6749, doi: 10.3390/molecules 28196749.

22 Yahya R, Al-Rajhi A M H and Alzaid S Z, Molecular docking and efficacy of aloe vera gel based on chitosan nanoparticles against *Helicobacter pylori* and its antioxidant and anti-inflammatory activities, *Polymers (Basel)*, 2022, 14(15), 2994, doi: 10.3390/polym14152994.

23 Girotra P, Thakur A, Kumar A and Singh S K, Identification of multi-targeted anti-migraine potential of nystatin and development of its brain targeted chitosan nanoformulation, *Int J Biol Macromol*, 2017, 96, 687-696, doi: 10.1016/j.ijbiomac.2016.12.065.

24 Mujtaba M A and Alotaibi N M, Chitosan-sodium alginate nanoparticle as a promising approach for oral delivery of rosuvastatin calcium: Formulation, optimization and *in vitro* characterization, *J Pharm Res Int*, 2020, 50-56, doi: 10.9734/jpri/2020/v32i130394.

25 Ali A, Ali A, Rahman M A, Warsi M H, Yusuf M, *et al.*, Development of nanogel loaded with lidocaine for wound-healing: Illustration of improved drug deposition and skin safety analysis, *Gels*, 2022, 8(8), 466, doi: 10.3390/gels8080466.

26 Khade S, Ambuskar S and Patil S, Nanosuspension-based formulation of *Alstonia scholaris* L.: *In vitro* evaluation for antidiabetic activity, *Bull Pharm Sci Assiut Univ*, 2026, doi: 10.21608/bfsa.2026.427229.2765.

27 Ho H M K, Craig D Q M and Day R M, Design of experiment approach to modeling the effects of formulation and drug loading on the structure and properties of therapeutic nanogels, *Mol Pharm*, 2022, 19(2), 602-615, doi: 10.1021/acs.molpharmaceut.1c00699.

28 Junyaprasert V B and Morakul B, Nanocrystals for enhancement of oral bioavailability of poorly water-soluble drugs, *Asian J Pharm Sci*, 2015, 10(1), 13-23, doi: 10.1016/j.ajps.2014.08.005.

29 Chalal S, Haddadine N, Bouslah N and Benaboura A, Preparation of Poly(acrylic acid)/silver nanocomposite by simultaneous polymerization–reduction approach for antimicrobial application, *J Polym Res*, 2012, 19(12), 24, doi: 10.1007/s10965-012-0024-1.

30 Ayazbayeva A Y, Shakhvorostov A V, Gussenov I S, Seilkhanov T M, Aseyev V O, *et al.*, Temperature and salt responsive amphoteric nanogels based on N-Isopropylacrylamide, 2-Acrylamido-2-methyl-1-propanesulfonic Acid Sodium Salt and (3-Acrylamidopropyl) Trimethylammonium Chloride, *Nanomaterials*, 2022, 12(14), 2343, doi: 10.3390/nano12142343.

31 Suhail M, Minhas M U and Naeem A, Preparation, characterization, *in-vitro* and toxicological evaluation of carbopol based nanogels for solubility enhancement of Valsartan, *Appl Surf Sci Adv*, 2023, 18, 100524, doi: 10.1016/j.apsadv.2023.100524.

32 Farooq U, Rasul A and Sher M, Development, characterization and evaluation of anti-fungal activity of miconazole based nanogel prepared from biodegradable polymer, *Pak J Pharm Sci*, 2020, 33(1(Special)), 449-457, doi: 10.36721/PJPS.2020.33.1.SP.449-457.1.

33 Obluchinskaya E D, Pozharitskaya O N and Shikov A N, *In vitro* anti-inflammatory activities of fucoidans from five species of brown seaweeds, *Mar Drugs*, 2022, 20(10), 606, doi: 10.3390/md20100606.

34 Djehiche C, Benzidane N and Djeghim H, Exploring the therapeutic potential of *Ammodaucus leucotrichus* seed extracts: A multi-faceted analysis of phytochemical composition, anti-inflammatory efficacy, predictive anti-arthritic properties, and molecular docking insights, *Pharmaceuticals*, 2024, 17(3), 385, doi: 10.3390/ph17030385.

35 Ahmad S, Saleem M and Riaz N, The natural polypeptides as significant elastase inhibitors, *Front Pharmacol*, 2020, 11, doi: 10.3389/fphar.2020.00688.

36 Pitz H da S, Pereira A and Blasius M B, *In vitro* evaluation of the antioxidant activity and wound healing properties of jaboticaba (*Plinia peruviana*) fruit peel hydroalcoholic extract, *Oxid Med Cell Longev*, 2016, 2016(1), doi: 10.1155/2016/3403586.

37 Balekar N, Katkam N G, Nakpheng T, Jehtae K and Srichana T, Evaluation of the wound healing potential of *Wedelia trilobata* (L.) leaves, *J Ethnopharmacol*, 2012, 141(3), 817-824, doi: 10.1016/j.jep.2012.03.019.

38 Alrasheid A A, Babiker M Y and Awad T A, Evaluation of certain medicinal plants compounds as new potential inhibitors of novel corona virus (COVID-19) using molecular docking analysis, *Silico Pharmacol*, 2021, 9(1), 10, doi: 10.1007/s40203-020-00073-8.

39 Nabi T, Riyed T H and Ornob A, Deep learning based predictive modeling to screen natural compounds against TNF-alpha for the potential management of rheumatoid arthritis: Virtual screening to comprehensive *in silico* investigation, *PLoS One*, 2024, 19(12), e0303954, doi: 10.1371/journal.pone.0303954.

40 Tipugade O, Sawale J and Jadhav N, Network pharmacology and molecular docking-based exploration of rubiaceous plants for breast cancer: Phytochemicals, preclinical studies, and regulatory perspectives, *Asian J Pharm Clin Res*, 2025, 52-71, doi: 10.22159/ajpcr.2025v18i7.54934.

41 Singh P, Singh V K and Singh A K, Molecular docking analysis of candidate compounds derived from medicinal plants with type 2 diabetes mellitus targets, *Bioinformation*, 2019, 15(3), 179-188, doi: 10.6026/97320630015179.

42 Adejoro I A, Babatunde D D and Tolufashe G F, Molecular docking and dynamic simulations of some medicinal plants compounds against SARS-CoV-2: an *in silico* study, *J Taibah Univ Sci*, 2020, 14(1), 1563-1570, doi: 10.1080/16583655.2020.1848049.

43 Tipugade O, Sawale J and Jadhav N, Unveiling the therapeutic potential of Nyctanthes arbor-tristis Linn. in breast cancer: A network pharmacology and molecular docking approach, *Fabad J Pharm Sci*, 2026, 51(1), 41-52, doi: 10.55262/fabadeczacilik.1786034.

44 Straksys A, Abouhagger A, Kirsnytė-Šniokė M, Kavleiskaja T, Stirke A, *et al.*, Development and characterization of a gelatin-based photoactive hydrogel for biomedical application, *J Funct Biomater*, 2025, 16(2), 43, doi: 10.3390/jfb16020043.

45 Sayyeda A, Ahmad Z, Ishtiaq S M, Irshad A, Shchinar S, *et al.*, Nanogel-based delivery of dequalinium chloride: A novel approach for antimicrobial and controlled drug release, *Naunyn Schmiedebergs Arch Pharmacol*, 2025, 398(11), 15561-15572, doi: 10.1007/s00210-025-04243-3.

46 Gonçalves R, Rabelo S, Teles A, do Rosário C J, Souza M, *et al.*, A thermoresponsive nanogel platform for controlled delivery of *Ageratum conyzoides* essential oil with improved stability and enhanced antimicrobial activity, 2026 doi: 10.2139/ssrn.6631353.

47 Yadav K, Sodhi R K and Sithta A, Albumin-stabilized *shorea robusta* resin nanoparticles embedded in a nanogel for improved controlled release and diabetic wound healing, *J Pharm Innov*, 2026, 21(2), 109, doi: 10.1007/s12247-025-10346-4.

48 Zucca G, Vigani B and Valentino C, Chondroitin sulphate-chitosan based nanogels loaded with naringenin-β-Cyclodextrin complex as potential tool for the treatment of diabetic retinopathy: a formulation study, *Int J Nanomed*, 2025, 20, 907-932, doi: 10.2147/IJN.S488507.

49 El-Messiry H, Atef N, Alaa E, Sherief D I and Fathy I A, Fish bone and chitosan based nanogels in green dentistry: sustainable and eco-friendly biomimetic remineralizing agents for early enamel caries, *BMC Oral Health*, 2026, 26(1), 632, doi: 10.1186/s12903-026-08008-z.

50 Ruiz-Ruiz J C, Matus-Basto A J, Acereto-Escoffié P and Segura-Campos M R, Antioxidant and anti-inflammatory activities of phenolic compounds isolated from Melipona beecheii honey, *Food Agric Immunol*, 2017, 28(6), 1424-1437, doi: 10.1080/09540105.2017.1347148.

51 Sen S, Chakraborty R, Maramsa N, Basak M and Deka B K D, *In vitro* anti-inflammatory activity of *Amaranthus caudatus* L. leaves, *Indian J Nat Prod Resour*, 2015, 6(4), 326-329,

52 Antunes J C, Domingues J M and Miranda C S, Bioactivity of chitosan-based particles loaded with plant-derived extracts for biomedical applications: emphasis on antimicrobial fiber-based systems, *Mar Drugs*, 2021, 19(7), 359, doi: 10.3390/md19070359.